proceedings

MDPI

Proceedings

$CuFe_2O_4$@CuO: A Magnetic Composite Synthesized by Ultrasound Irradiation and Degradation of Methylene Blue on Its Surface in the Presence of Sunlight †

Ahmad Massoud-Sharifi, Gheffar K. Kara and Mahboubeh Rabbani *

Department of Chemistry, Iran University of Science and Technology, Narmak, Tehran 16846-13114, Iran; Massoud.sharifi85@gmail.com (A.M.-S.); gheffar.kara@gmail.com (G.K.K.)

* Correspondence: m_rabani@iust.ac.ir; Tel.: +98-21-77240651

† Presented at the 4th International Electronic Conference on Water Sciences, 13–29 November 2019; Available online: https://ecws-4.sciforum.net/.

Published: 12 November 2019

Abstract: Spinel ferrite MFe_2O_4 (M = Cu, Ca, Mg, Ni, etc.) nanoparticles and their composites are a new promising materialbecause they have shown great interest in the field of sensing, optoelectronics, catalysis, and solar cells due to their unique physical and chemical properties that differ from their bulk structures. Today, lots of $CuFe_2O_4$ nanomaterials have been synthesized by different methods, such as hydrothermal route and sol-gel combustion methods. Nevertheless, there are hardly any results about photocatalytic activity. For this reason, we tried to increase optical properties by preparing a composite of $CuFe_2O_4$ nanomaterials with other oxides. In this paper, a $CuFe_2O_4$@CuO magnetic composite was synthesized via an ultrasound method. The samples prepared were characterized by X-ray diffraction (XRD), Fourier-transform infrared spectroscopy (FT-IR), diffuse reflectance spectrpscopy (DRS), field emission scanning electron microscopy (FESEM) images, vibrating sample magnetometer (VSM), and elemental analysis (energy-dispersive X-ray (EDX)). The catalytic activity of as-synthesized $CuFe_2O_4$@CuO was evaluated using the degradation of methylene blue. Furthermore, a possible reaction mechanism was discussed. Finally, the catalyst was used for effective degradation of methylene blue (MB) in its solution, which indicated a potential for practical applications in water pollutant removal and environmental remediation.

Keywords: $CuFe_2O_4$@CuO; nanocomposite; methylene blue; photodegradation

1. Introduction

In the last few years, metallic oxides and their mixed compounds (as called composites) have been considered as a green semiconductor photocatalyst to resolve the increasing energy and environmental crisis by using solar light sources for organic dye degradation and hydrogen generation from water [1–5]. When the single-component photocatalysts have a poor quantum efficiency and low photocatalytic performance, they are mixed with each other and a heterojunction-type photocatalytic system is created. In recent years, this system has been used as part of an important strategy to overcome the drawbacks of a single photocatalyst, which modifies the yield of the photoexcited (electron-holes) separation [6,7]. Unfortunately, one of the disadvantages of these heterojunction systems is that the generation of the electron-hole pair is ordinarily weakened after a charge transfer [8]. Therefore, the high charge-separation efficiency and strong redox ability are difficult to possess at the same time. Recently, the concentration of a photocatalytic system with

magnetic properties is an ideal and effective means because it not only can reduce the bulk electron-hole recombination and preserved redox ability but it is also a green material [9].

Copper ferrites have been continuously investigated because of their properties (semiconducting, magnetic properties, thermal, and chemical stabilities). Nanosized copper spinel ferrite can be fabricated by a variety of methods such as ball-milling [10], sol-gel [11], and co-precipitation [12].

Copper oxide nanoparticles have attracted a lot of attention in various fields, particularly catalytic applications, because they possess appealing properties like non-toxicity, chemical stability, electrochemical activity, etc. Multiple morphologies and sizes of CuO nanoparticles have been synthesized by using different synthetic methods such as thermal evaporation, thermal decomposition, thermal oxidation, electrospinning, solid-liquid arc discharge processes, chemical vapor deposition, sol-gel method, etc. [13].

In this context, a magnetic composite ($CuFe_2O_4$@CuO) was prepared via ultrasound irradiation in the presence of ammonia solution and ethylene glycol. Also, we report on the photocatalytic degradation of methylene blue (MB) over $CuFe_2O_4$@CuO heterojunctions under visible light irradiation.

2. Results and Discussion

All as-prepared samples were characterized by X-ray diffraction (XRD), field emission scanning electron microscopy (FESEM) images, energy-dispersive X-ray (EDX), Fourier-transform infrared spectroscopy (FT-IR), UV-Vis, diffuse reflectance spectrpscopy (DRS) and vibrating sample magnetometer (VSM) techniques.

2.1. XRD Patterns

Figure 1A–C shows the XRD pattern of the $CuFe_2O_4$@CuO photocatalysts that contained pure CuO and $CuFe_2O_4$. The X-ray diffraction pattern of the $CuFe_2O_4$ (Figure 1A) introduced several intense diffraction 2θ angles at 19.32, 30.92, 36.68, 42.84, 51.2, 54.4, 58.12, 63.4, and 75.04°, respectively (JCPDS card No. 01-077-0010) [13].

To identify the crystallinity and crystal phases of the CuO pearls, XRD analysis was performed and is shown in Figure 1B. Upon notification reflection peaks, only a pure monoclinic phase of CuO is presented in the prepared nanoparticles, which are in good agreement with the literature value (JCPDS card No. 05-0661).

XRD pattern for the magnetic composite (CuO@$CuFe_2O_4$) sample synthesized with ultrasound power and calcination temperature is depicted in Figure 1C. It is noted in this pattern that whole peaks are in accordance with the corresponding standard pattern of copper ferrite and the standard pattern of copper oxide, which confirm the presence of each one in the as-prepared composite.

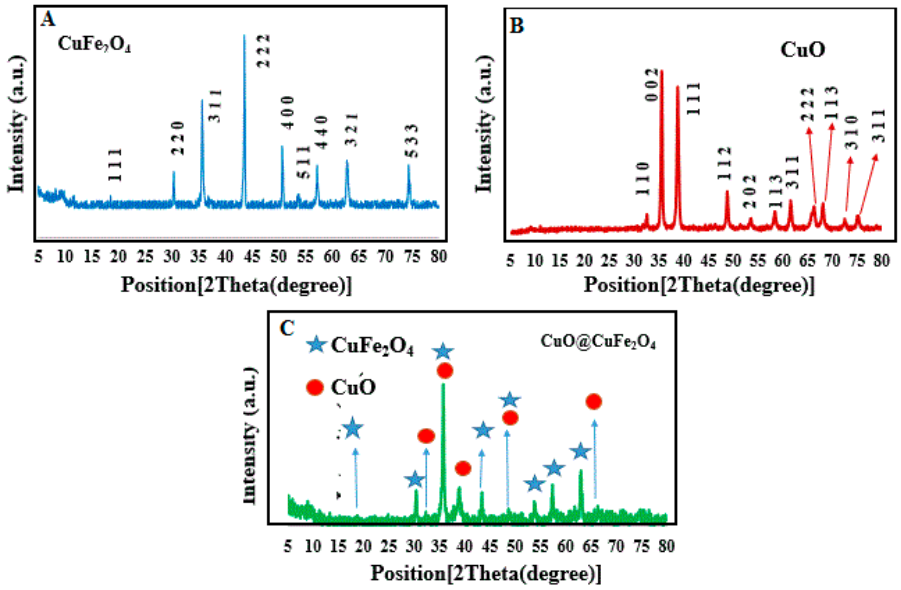

Figure 1. X-ray diffraction patterns of (**A**) $CuFe_2O_4$, (**B**) CuO, and (**C**) $CuO@CuFe_2O_4$.

2.2. FT-IR Study

The FT-IR transmission mode spectrum for everything synthesized ($CuFe_2O_4$, CuO, and $CuO@CuFe_2O_4$) was studied, as shown in Figure 2. According to the results, there is no observed additional adsorption peaks of each spectrum that indicates the presence of any byproduct or raw organic material used for the preparation. The existence of CO_2 molecule over a compound's surface was verified by the weak absorption peak observed around 2333.43 cm^{-1}.

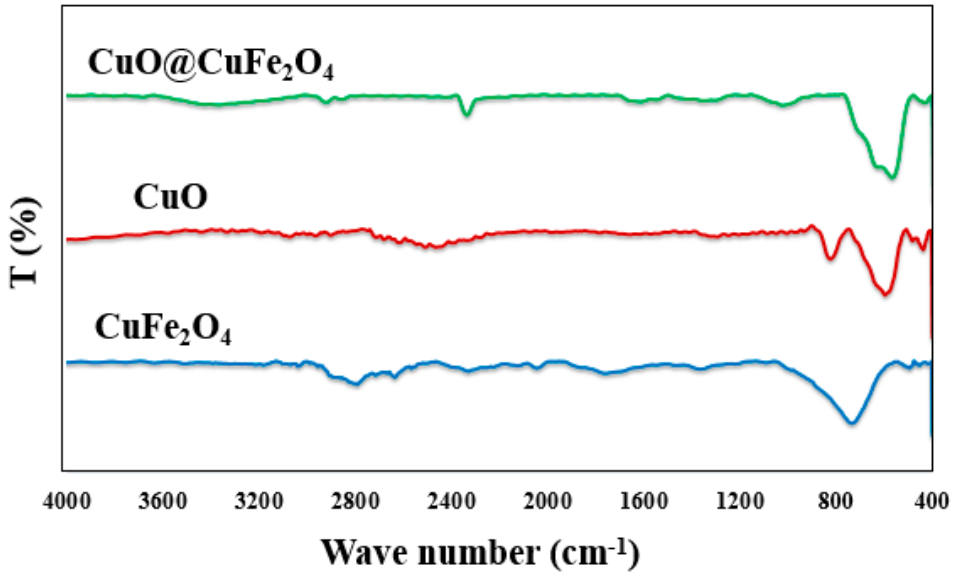

Figure 2. Fourier-transform infrared spectra for all synthesized samples.

2.3. Morphological Analysis of $CuFe_2O_4$, CuO and Their Composite

The FESEM micrograph of $CuFe_2O_4$ nanospheres that grew under solvothermal conditions is shown in Figure 3A,B. These particles have a sphere-like structure with an approximate average size of 170–195 nm. Further, the homogeneous distribution of copper ferrite nanospheres has led to enhancing the density of its surface. The aggregation of the copper ferrite nanosphere is not large. Figure 3C,D shows the structural morphology of the CuO nanostructure that was prepared via pyrolysis/hydrolysis of copper (II) nitrate in an ethylene glycol/ammonia solution with ultrasound

irradiation in ambient air. The morphology of these synthesized particles were pearl with a smooth surface. Average particle size varied fin 25–35 nm range. Figure 3E,F reveals the FESEM image of the typical CuO@$CuFe_2O_4$ magnetic composite. These images confirmed that the morphological structure of the product is close to spherical but not uniform with various sizes. Moreover, there are agglomerated particles in some sites, which can be attributed to many factors (i.e., high annealing temperature, the presence of electrostatic, and Van der Waals forces between magnetic particles). In addition, it was noted that a number of small nanoparticles of copper oxide uniformly covered the surfaces of $CuFe_2O_4$ on a large scale (~310 nm).

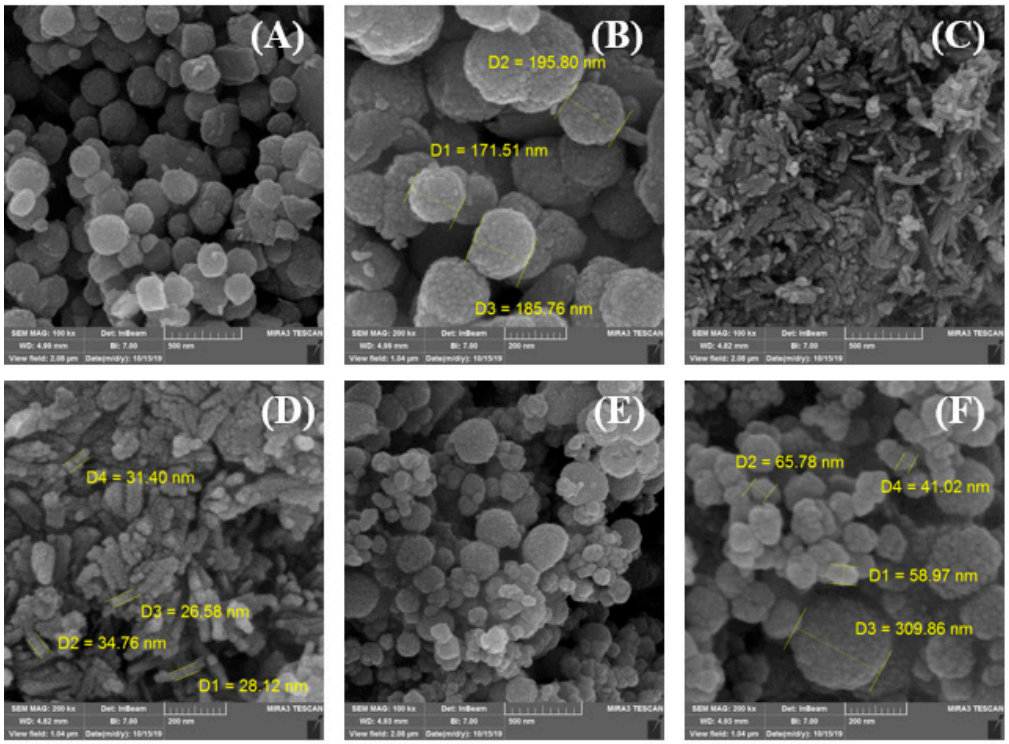

Figure 3. Field emission scanning electron microscopy images of (**A**,**B**) $CuFe_2O_4$, (**C**,**D**) CuO and (**E**,**F**) CuO@$CuFe_2O_4$.

2.4. Elemental Analysis

The composition analysis of CuO@$CuFe_2O_4$ was examined through an energy dispersive analysis (EDX) spectrum, as depicted in Figure 4 which confirms the existence of O, Fe, and Cu elements. The atomic percentage of the elements is nearly close to stoichiometry value. The experimental values of the atomic percentage have some copper insufficiency.

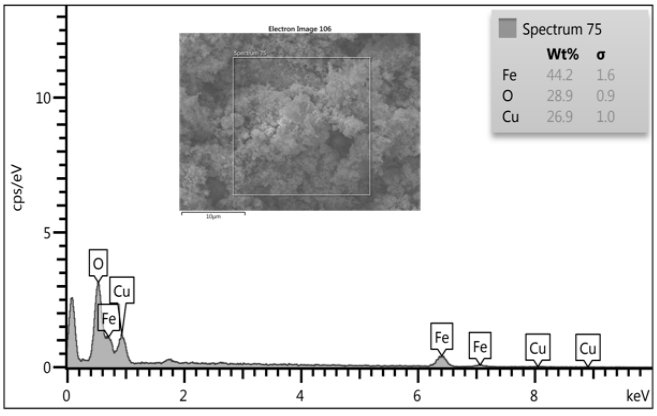

Figure 4. Energy dispersive analysis (EDX) spectrum of CuO@$CuFe_2O_4$.

2.5. VSM Analysis

The hysteresis loop of $CuFe_2O_4$ and $CuO@CuFe_2O_4$ nanoparticles is shown in Figure 5A,B. The saturation magnetization values of $CuO@CuFe_2O_4$ were found to be lower than the corresponding $CuFe_2O_4$. The value of saturation magnetization values of $CuFe_2O_4$ (Ms = 86.41 emu/g) is compared to that of $CuO@CuFe_2O_4$ (Ms = 72.58 emu/g) and can be expressed in the basis of a homogeneous covering model that explains the narrow distribution of densely covered CuO on copper ferrite surfaces that resulted in reducing magnetization. Moreover, the magnetic moment was reduced by increasing the particles size and sintering the temperature.

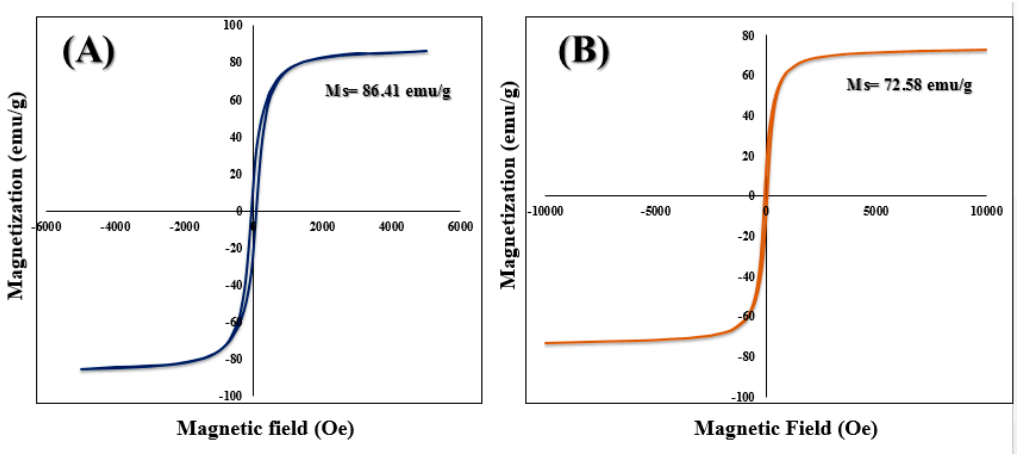

Figure 5. Magnetic measurements of (**A**) $CuFe_2O_4$ and (**B**) $CuO@CuFe_2O_4$.

2.6. Photocatalytic Activity

The photocatalytic activity of pure oxides and $CuO@CuFe_2O_4$ catalysts under sunlight irradiation was defined by measuring the photodegradation of methylene blue (MB) aqueous solutions. Methylene blue (MB) is a cationic dye with a methyl nitride group [$(CH3)_2N^+$]. Figure 6A,B illustrates the comparison of the photocatalytic activity of $CuFe_2O_4$, CuO, and $CuO@CuFe_2O_4$ composite for the degradation of methylene blue (MB) (10 mg L^{-1}) under sunlight irradiation for 3 h. In order to investigate the adsorption properties for the photocatalysts, its working in dark was tested. Under sunlight irradiation, the results show that the degradation yield of methylene blue (MB) in the presence of CuO, $CuFe_2O_4$, and $CuO@CuFe_2O_4$ samples was 18%, 36%, and 90%, respectively. However, these values were 8% (CuO), 13% ($CuFe_2O_4$), and 42% composite in the dark (Figure 6B). Thus, the $CuO@CuFe_2O_4$ composite displays a better degradation performance of methylene blue (MB) rather than pure oxides in the same condition. Surprisingly, pristine CuO was very low and had sluggish degradation behavior, which can be attributed to the very recombination rates of (electron-hole) pairs in pure oxides and also the absence of the second material, such as copper ferrite for a charge transfer. However, the adsorption results for samples were also not credible.

Moreover, Figure 7 displays the comparison of the methylene blue (MB) removal yield in various times. $CuO@CuFe_2O_4$ was under sunlight irradiation and in dark. The obtained results illustrate that the MB decomposed 90% in 120 min under sunlight irradiation and was adsorbed only 42% after 90 min in the dark. Therefore, the final composite is as an excellent photocatalyst for degradation of the dye under sunlight irradiation.

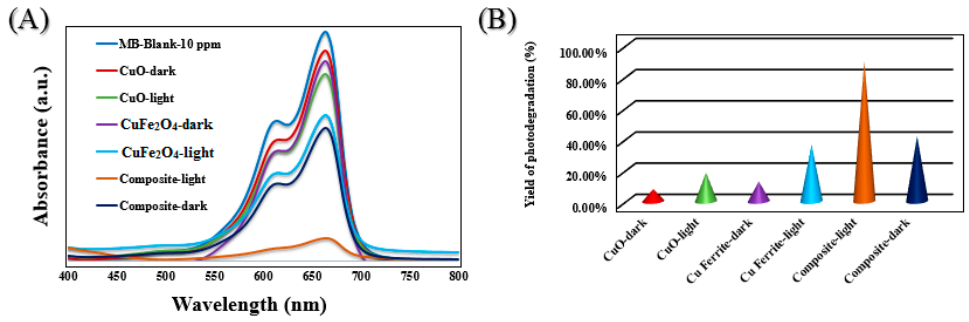

Figure 6. (**A**) Photocatalytic degradation of methylene blue (MB) (initial concentration: 10 mg·L^{-1}, 10 mL) using pure oxides and their composite under sunlight irradiation; (**B**) efficiency of degradation in 180 min.

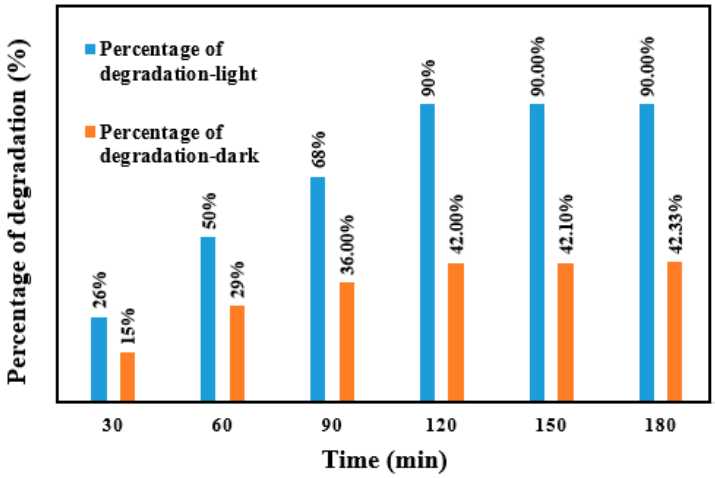

Figure 7. Percentage degree of methylene blue (MB) photodegradation in the presence of prepared samples under visible-light and dark conditions in various times.

3. Materials and Methods

3.1. Preparation of the CuO@CuFe$_2$O$_4$ Nanocomposite

Firstly, 0.12 g of $FeCl_3 \cdot 6H_2O$ and 0.0511 g of $CuCl_2 \cdot 2H_2O$ were added into 15 mL of an ethylene glycol (EG) solution. Then, 0.2 g of ammonium acetate (CH_3COONH_4) was added into the mixture under vigorous stirring. This solution was sonicated for 30 min. Subsequently, the homogenous mixture was transferred into a Teflon-lined stainless-steel autoclave with 40 mL capacity and heated at 200 °C for 20 h.

A solid powder of the CuO@CuFe$_2$O$_4$ nanocomposite was synthesized using an ultrasound method under an ambient condition. Next, 0.525 g of copper ferrite and 5 mL of ethylene glycol were well-mixed and sonicated for 25 min using an ultrasonic. Afterward, 0.575 g of copper nitrate ($Cu(NO_3)_2 \cdot H_2O$) was dissolved into 25 mL of DI H_2O and was slowly dispersed into the copper ferrite/EG mixture. During sonication, 15 mL of ammonia solution (25%) was added to adjust the pH to 11. After sonication, the product was gathered by centrifugation and washed by ethanol and deionized water (DI), which removed any organic materials that adsorbed on the surface. After that, the nanocomposite was dried at 70 °C, pinpointed in crucible, and calcined at 200 °C for 2 h.

3.2. Photocatalytic Experiments

Photocatalytic activity of the prepared CuFe$_2$O$_4$ nanospheres, CuO nanopearls, and CuO@CuFe$_2$O$_4$ magnetic composite was evaluated with photodegradation of MB solutions. In the experimental set-up, 0.01 g of photocatalyst was added to a 100 mL photoreactor containing 10 mL

of MB dye (10 mg·L^{-1}). In order to obtain an equilibrium point for the initial physical adsorption of MB over the sample surface, the solution was stirred in the dark for 30 min. Then, the container was placed under sunlight for about 3 h. All photocatalytic experiments were carried out in the same conditions. The percentage of removal efficiency (X%) is given by:

$$X\% = \frac{C - C_0}{C_0} \times 100 \quad (1)$$

where C_0 is the concentration of dye at 0 minute and C is the concentration of dye at time t.

4. Conclusions

A superparamagnetic CuO@$CuFe_2O_4$ composite with spherical morphology was successfully synthesized with low-cost precursors and a simple sonication technique. The improved catalytic activity of CuO@$CuFe_2O_4$ was explored on the basis of a tailored band gap and chemical interaction between $CuFe_2O_4$ and CuO, leading to a fast charge transport through the interfacial layers. This inhibited the charge recombination (e-/h+ pairs) and ensured accessibility for free charge carriers to support the catalytic activity. Room temperature magnetization outcomes revealed a superparamagnetic behavior of the as-synthesized $CuFe_2O_4$ and CuO@$CuFe_2O_4$, indicating that this nanocomposite can be a usable photocatalyst due to its efficient magnetic separation.

References

1. Greene, D.; Serrano-Garcia, R.; Govan, J.; Gun'ko, Y. Synthesis characterization and photocatalytic studies of cobalt ferrite-silica-titania nanocomposites. *Nanomaterials* **2014**, *4*, 331–343.
2. Comini, E.; Sberveglieri, G.; Ferroni, M.; Guidi, V.; Martinelli, G. Response to ethanol of thin films based on Mo and Ti oxides deposited by sputtering. *Sens. Actuators B Chem.* **2003**, *93*, 409–415.
3. Kasemr, K.K.; Rameyl, H.; Ahmed, V. Photo-Electrochemical Studies on TiO_2-Doped Ce (III/IV) Oxides Nanoparticles in Aqueous Electrolytes. *Mater. Sci. Appl.* **2013**, *4*, 637, doi:10.4236/msa.2013.410078.
4. Carnes, C.L.; Klabunde, K.J. Unique chemical reactivities of nanocrystalline metal oxides toward hydrogen sulfide. *Chem. Mater.* **2002**, *14*, 1806–1811.
5. Rahimi, R.; Zargari, S.; Yousefi, A.; Berijani, M.Y.; Ghaffarinejad, A.; Morsali, A. Visible light photocatalytic disinfection of *E. coli* with TiO_2-graphene nanocomposite sensitized with tetrakis (4-carboxyphenyl) porphyrin. *Appl. Surf. Sci.* **2015**, *355*, 1098–1106.
6. Weckhuysen, B.M. Snapshots of a working catalyst: Possibilities and limitations of in situ spectroscopy in the field of heterogeneous catalysis. *Chem. Commun.* **2002**, 97–110, doi:10.1039/b107686h.
7. Zhao, J.; Yang, X. Photocatalytic oxidation for indoor air purification: A literature review. *Build. Environ.* **2003**, *38*, 645–654.
8. Zhu, Y.P.; Ren, T.Z.; Ma, T.Y.; Yuan, Z.Y. Hierarchical structures from inorganic nanocrystal self-assembly for photoenergy utilization. *Int. J. Photoenergy* **2014**, doi:10.1155/2014/498540.
9. Pullar, R.C. Hexagonal ferrites: A review of the synthesis, properties and applications of hexaferrite ceramics. *Prog. Mater. Sci.* **2012**, *57*, 1191–1334.
10. Jiang, J.Z.; Goya, G.F.; Rechenberg, H.R. Magnetic properties of nanostructured $CuFe_2O_4$. *J. Phys. Condensed Matter* **1999**, *11*, 4063, doi:10.1088/0953-8984/11/20/313/meta.
11. Liu, X.Q.; Tao, S.W.; Shen, Y.S. Preparation and characterization of nanocrystalline α-Fe_2O_3 by a sol-gel process. *Sens. Actuators B Chem.* **1997**, *40*, 161–165.
12. Pandya, P.B.; Joshi, H.H.; Kulkarni, R.G. Magnetic and structural properties of $CuFe_2O_4$ prepared by the co-precipitation method. *J. Mater. Sci. Lett.* **1991**, *10*, 474–476.
13. Verma, A.; Jaihindh, D.P.; Fu, Y.P. Photocatalytic 4-nitrophenol degradation and oxygen evolution reaction in CuO/gC_3N_4 composites prepared by deep eutectic solvent-assisted chlorine doping. *Dalton Trans.* **2019**, doi:10.1039/C9DT01046G.